Very low noise AC/DC power supply systems for large detector arrays

C. Arnaboldi, A. Baù, P. Carniti, L. Cassina, A. Giachero, C. Gotti, M. Maino, A. Passerini, and G. Pessina

---

Articles you may be interested in

A highly stable DC power supply for precision magnetic field measurements and other purposes
Rev. Sci. Instrum. **83**, 045101 (2012); 10.1063/1.3698208

Highly efficient pulsed power supply system with a two-stage LC generator and a step-up transformer for fast capillary discharge soft x-ray laser at shorter wavelength
Rev. Sci. Instrum. **81**, 013303 (2010); 10.1063/1.3276705

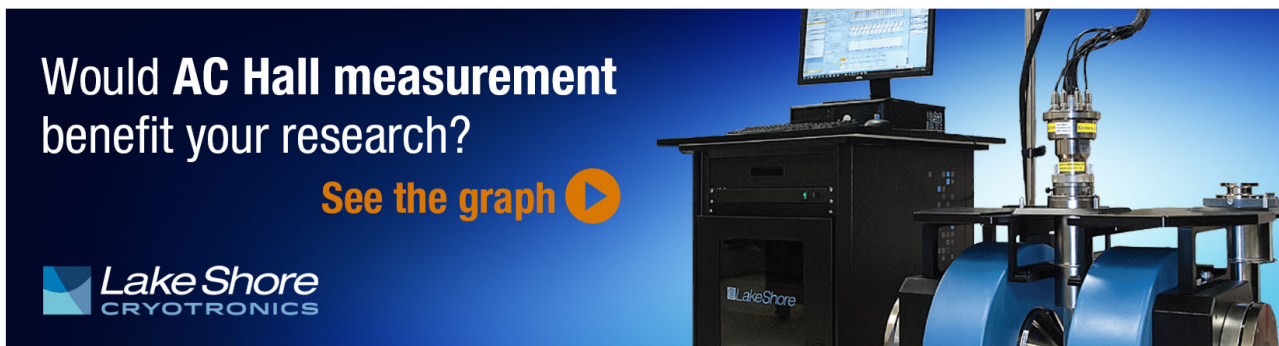A New Device for Bimorph Mirrors Technology: the A1902BS Bipolar Power Supply System
AIP Conf. Proc. **879**, 683 (2007); 10.1063/1.2436154

Development of battery powered 100 kV dc power supply
Rev. Sci. Instrum. **77**, 106104 (2006); 10.1063/1.2362721

Low-noise, low drift, high precision linear bipolar (±10 V) voltage supply/reference for cryogenic front-end apparatus
Rev. Sci. Instrum. **70**, 3473 (1999); 10.1063/1.1149939

Very low noise AC/DC power supply systems for large detector arrays

C. Arnaboldi,[1,2] A. Baù,[1,2] P. Carniti,[1,2] L. Cassina,[1,2] A. Giachero,[1,2] C. Gotti,[1,2,a)]
M. Maino,[1,2] A. Passerini,[1,2] and G. Pessina[1,2]

[1]*INFN, Istituto Nazionale di Fisica Nucleare Sezione di Milano Bicocca, Piazza della Scienza 3, Milano I-20126, Italy*
[2]*Dipartimento di Fisica, Università di Milano Bicocca, Piazza della Scienza 3, Milano I-20126, Italy*

In this work, we present the first part of the power supply system for the CUORE and LUCIFER arrays of bolometric detectors. For CUORE, it consists of AC/DC commercial power supplies (0–60 V output) followed by custom DC/DC modules (48 V input, ±5 V to ±13.5 V outputs). Each module has 3 floating and independently configurable output voltages. In LUCIFER, the AC/DC + DC/DC stages are combined into a commercial medium-power AC/DC source. At the outputs of both setups, we introduced filters with the aim of lowering the noise and to protect the following stages from high voltage spikes that can be generated by the energy stored in the cables after the release of accidental short circuits. Output noise is very low, as required: in the 100 MHz bandwidth the RMS level is about 37 μV_{RMS} (CUORE setup) and 90 μV_{RMS} (LUCIFER setup) at a load of 7 A, with a negligible dependence on the load current. Even more importantly, high frequency switching disturbances are almost completely suppressed. The efficiency of both systems is above 85%. Both systems are completely programmable and monitored via CAN bus (optically coupled). © *2015 AIP Publishing LLC.* [http://dx.doi.org/10.1063/1.4936269]

I. INTRODUCTION

CUORE[1,2] and LUCIFER[3] are two experiments designed to study the neutrinoless double beta ($0\nu\beta\beta$) decay of ^{130}Te and ^{82}Se, respectively, with bolometric techniques. The two crystal arrays will be cooled down to cryogenic temperatures, around 10 mK. Imping particles will produce thermal signals in CUORE, and thermal and light signals in LUCIFER, where the dual readout will be used to suppress background.

Double beta decays are very rare processes. To maximize sensitivity, both CUORE and LUCIFER will take data for several years and are required to be very stable. The conversion gain between energy and voltage of cryogenic bolometers strongly depends on their bias voltages and to preserve the detector energy resolution and produce consistent data, the front-end electronics must exhibit very low noise, below 10 nV/$\sqrt{\text{Hz}}$ down to 1 Hz, and very low drift, below ±1 ppm/°C. Although the front-end electronics have a good degree of tolerance to noise injected from the power supplies, a larger safety margin for system operation is achieved if the Power Supply System is designed to be stable and clean.

The power supply system designed to achieve these goals is composed by several units having four stages each for CUORE that foresees about 1000 channels: the first stage of each unit is a commercial AC/DC and the second is a set of custom DC/DC modules. The fourth and final elements of each unit are very low noise and very low drift linear power supplies[4] that are an updated version of a device already designed and produced for the previous CUORICINO experiment.[5] Before the fourth stage are the protection/filter modules that

constitute the third stage. The efficiency of our protection/filter modules allows to obtain a very low noise at the input of the fourth stage for both setups. The purpose of each DC/DC unit is to provide 3.3 V or 5 V lines for the digital circuitry and pairs of bipolar supplies adjustable from ±5 V to ±13.5 V for the analogue circuitry. LUCIFER will have about 100 channels and will need only one unit, for which the choice was to merge the first 2 stages in a medium-power commercial AC/DC.

In this paper, the first three stages of the power supply chain will be presented. Noise results and characterization of the production of the DC/DC modules for CUORE and LUCIFER will be shown in detail. For details on the fourth stage, we instead refer to other papers.[4,5]

II. THE POWER SUPPLY SYSTEM

The power supply system for CUORE consists of five units, each composed as shown in Figure 1. Each unit can source enough current to power the entire readout chains of 200 channels, from the front-end amplifiers to the active anti-aliasing filters located just before the DAQ. The AC/DC commercial power supply (TDK-Lambda Genesys Series 60-25, up to 60 V, 25 A output) is set to 48 V and is followed by six custom DC/DC modules (±12 V, 150 W). Each DC/DC module is laid out on a two-layer 220×236 mm^2 PCB (Euro-card standard), called power slot from now on, having 3 output channels. The six power slots are accommodated in a standard 19 in. crate. Each power slot drives two linear power supplies located at the end of 10 m connecting cables. Just before each linear power supply is a protection/filter circuit. The linear power supplies are the last stage of the CUORE power supply system and are located close to the front-end, inside a Faraday
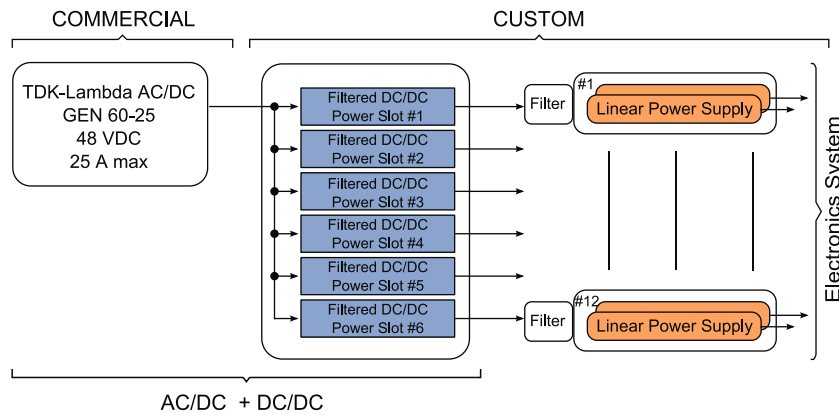
a)claudio.gotti@mib.infn.it

FIG. 1. Block diagram of a complete unit of the CUORE power supply system. The AC/DC system is a TDK-Lambda that supplies 6 custom DC/DC modules. Each DC/DC module supplies 2 low noise and low drift Linear power supplies.

cage. They are used to set the final voltages to a precise value, stabilized against fluctuations in temperature and with very low noise.

In the CUORE setup, the total load of each power slot is about 15 A. For a typical output voltage of 6.5 V, this results in 100 W per DC/DC. Considering, as a worst case, an efficiency of the DC/DCs of 75%, the power that the AC/DC modules must source is 800 W. The AC/DC modules are therefore set to 48 V and source about 16 A, well below their rated limit of 25 A. This estimate already includes a safety margin since the actual efficiency of the DC/DC modules is higher than 75%. LUCIFER only needs one pair of linear power supplies; therefore, a medium-power AC/DC (Rohde & Schwarz HMP4040) is enough for the block AC/DC + DC/DC of Figure 1.

A. Power slot stage

The custom part of the AC/DC + DC/DC block of Figure 1 is the six power slots, whose block diagram is shown in Figure 2. The power slot has three independent channels, each based on a commercial 48 V input DC/DC module from Vicor, the V48C12C150BL. This series of devices from Vicor is based on variable-frequency, quasi-resonant, zero-Current switch, zero-Voltage switch modulators, designed to minimize the inrush currents and noise.[6-9] Each DC/DC is cascaded by an active filter, Vicor μRAM, designed to attenuate the switching noise by more than 40 dB.[10]

The 48 V input voltage is common to the 3 DC/DC converters in each Power Slot, but their output voltages are
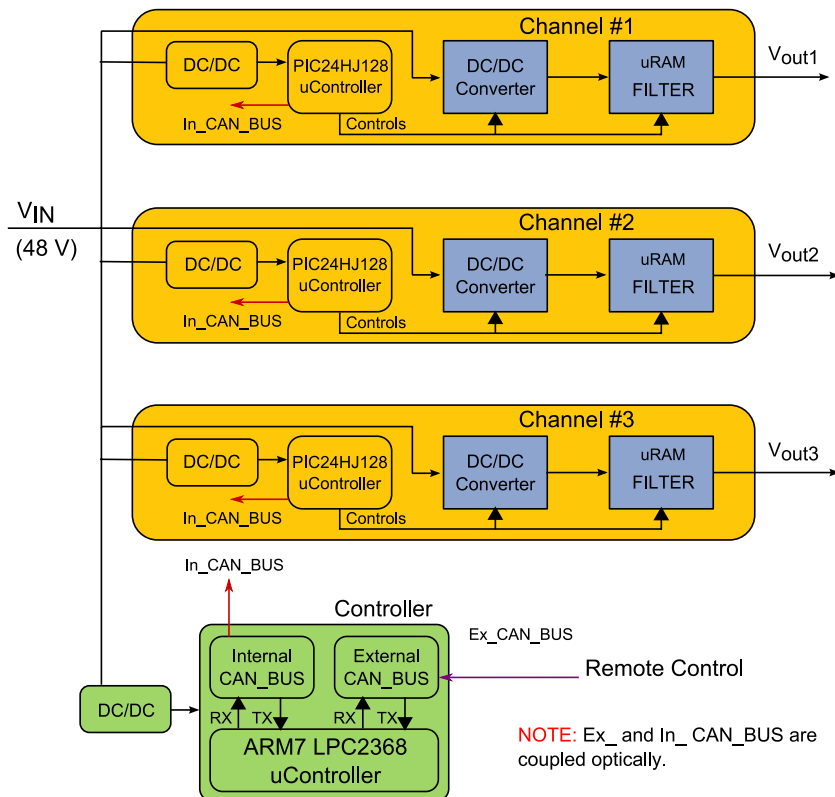

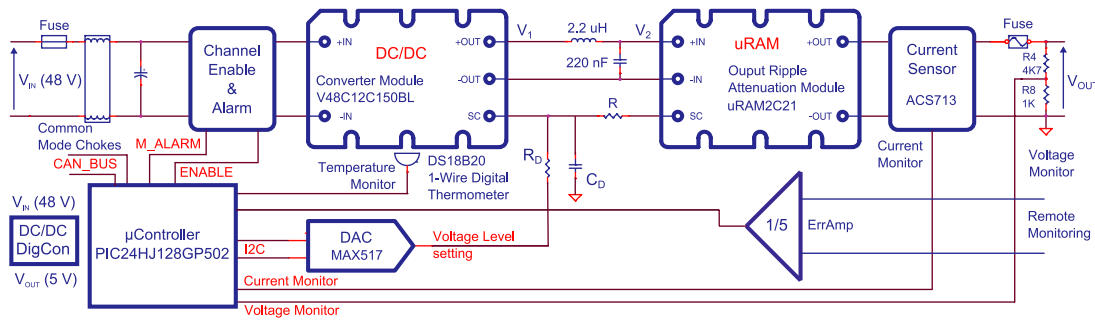FIG. 2. Schematic diagram of the DC/DC power slot.

FIG. 3. Schematic details of a channel in the power slot.

isolated from each other. Each channel is managed by its own control system based on a μcontroller, supplied by a dedicated low power DC/DC. The communication between the onboard μcontrollers is through a private CAN bus that is implemented via digital opto-couplers, a set for each μcontroller. A fourth μcontroller, on a separate small board, collects data from the internal CAN bus and communicates with external control systems with a wide area CAN bus link. This last μcontroller is biased with an additional low power DC/DC converter to preserve isolation.

More details about the circuit topology of one of the 3 channels of the power slot are given in Figure 3 where 2 separate sub-systems are distinguishable. The 48 V input voltage is connected to the DC/DC module (V48C12C150BL) through the "Channel Enable & Alarm" block that is composed of a few optical transistors with which it is possible to enable or inhibit the channel and read back digital alarms such as over temperature and voltage, from the DC/DC module. The DC/DC module is cascaded by the active μRAM filter which feeds the output through the Hall current sensor ACS713 from Allegro MicroSystems.

The 48 V input voltage is also connected to the "DC/DC DigCon" block, a low power regulator which provides the 5 V voltage level for the on-board control circuits, and is cascaded by linear regulators to provide also 3.3 V. The common ground between the power chain and the controlling circuitry is only at the output node.

The μcontrollers on the power slot are the 16 bit PIC24HJ-128GP502 from microchip. The copper thickness of the PCB is 100 μm (3.0 oz) in order to present a low impedance to large currents. Such copper thickness does not allow small clearance between pins of integrated circuits; therefore, package families such as TQFP cannot be used. The PIC24HJ128GP502 with its 28-pins SOIC package (1.27 mm lead pitch) is perfect in this case. The LPC2368 (full code LPC2368FBD100), having 2 CAN bus peripherals, is instead packaged in a 100-pins TQFP (0.5 mm lead pitch) and sits on its own PCB having standard 18 μm (0.5 oz) copper thickness.

The main intelligent functions to mention are the monitoring of the output voltage, output current, and temperature. The temperature is read with a one-wire thermometer thermally anchored to the heat sink on the top of the DC/DC. The ADCs on the PIC24HJ128GP502 are used to monitor the output voltage, taken at the R_4, R_8 attenuator, and the voltage proportional to the output current from the ACS713 current sensor.

By means of a 8 bit DAC and resistor R_D (330 Ω), it is possible to set the output voltage from a few V up to 13.5 V. Capacitor C_D (1000 μF) is used to filter the low frequency noise from the DAC that would otherwise be injected at this reference node.

The block "ErrAmp" allows remote voltage regulation. It attenuates by 5 the voltage of the relevant nodes and is read by one of the ADCs (12 bits) of the μcontroller. In this way, the remote regulation is digital and can be done at a proper, selectable rate.

An interlock, not shown, is also included. The interlock is common to the 3 channels of the Power Slot and is managed by the main μcontroller.

In Figure 4 a picture of the Power slot is shown. Each DC/DC module and its corresponding μRAM filter have their own heat sink on top.

B. Protection/filter stage

Among the figures of merit of a power supply system is not only its conducted noise but also its electromagnetic interference (EMI) emissions. The AC/DC is therefore located far from the detectors and front-end electronics and has its 48 V output voltage floating. The DC/DC is closer to the detector area, but outside the Faraday Cage that protects the experiment, and has its outputs floating as well. Finally, the linear power supply is the last stage that supplies the front-end and shares with it the ground potential. The distances from the AC/DC to the DC/DC and from the DC/DC to the front-end are about 10 m each. We developed special connecting cables for this having six power conductors with 6 mm^2 section and two smaller wires for the interlock, all shielded with a custom tubular copper mesh.

A first important aspect that regards long connecting cables is safety. We measured a few cables and found, in average, an inductance of about 0.7 μH/m when the cables were laid out straight. The inductance increased by up to about 3–4 times if the cables were coiled. A significant amount of energy is therefore stored and freed, in the form of a voltage spike, after the release of an accidental short circuit at the end of a long cable, like our 10 m cable. In Figure 5, an example of what can happen is shown: at the beginning, the nominal output voltage is 8 V but the output is shorted to ground. The current is limited to 20 A. When the short is released a 20 V, 10 μs spike is generated, with a faster peak in excess of 90 V.
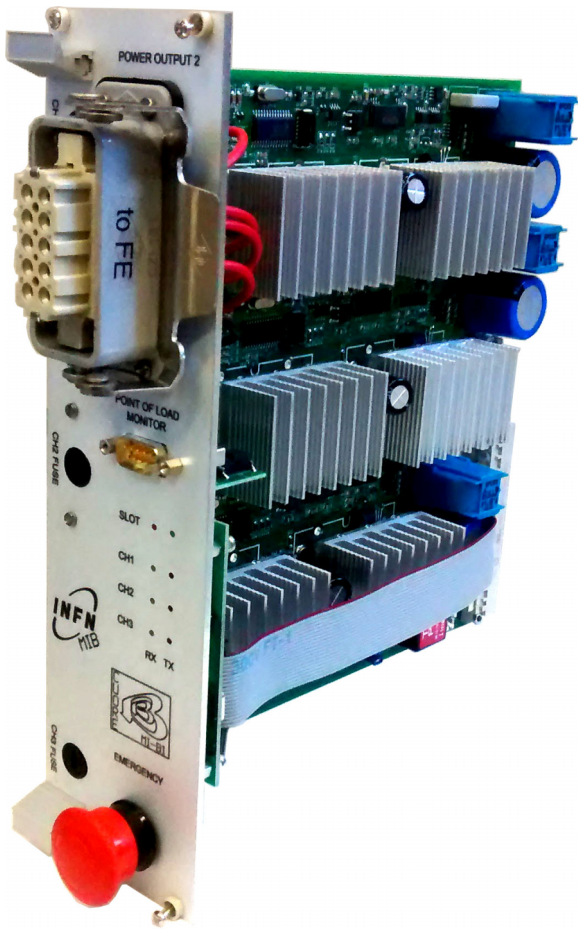
FIG. 4. Photograph of the power slot module.

Voltage suppressors are commonly used to limit high voltage transients. They are good devices, but not very precise in the tripping voltage. Other solutions make use of Zener diodes. We have implemented a very simple solution that is able to filter the line and protect the load at the same time. The solution is based on the following equation, valid when at the end of the cable a capacitance C_{Lim} is connected,
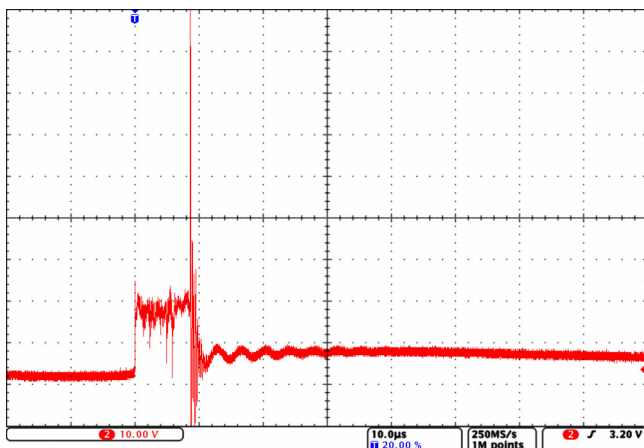

FIG. 5. Signal at the end of a 10 m cable after the release of an accidental short circuit. Vertical scale is 10 V/div, horizontal scale is 10 μs/div. The nominal DC value is 8 V, while the voltage peak is larger than 90 V.
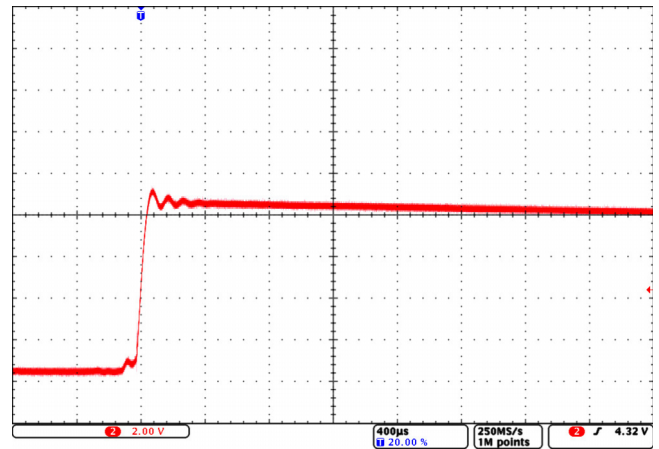

FIG. 6. Signal at the end of a 10 m cable, to which a protecting capacitor is connected, after the release of an accidental short circuit. Vertical scale is 2 V/div, horizontal scale is 400 μs/div. The nominal DC value is 8 V: the over-voltage is now negligible.

$$\frac{1}{2} C_{Lim} \cdot V_{Over}^2 = \frac{1}{2} L_{Cable} \cdot I_{Short}^2. \tag{1}$$

The energy stored in the cable is then shared between the inductance of the cable L_{Cable} and the capacitance C_{Lim}, but the voltage spike is limited to V_{Over}. Once the short circuit current I_{Short} is known and the maximum allowed overvoltage is given, from (1) we can calculate the minimum value of C_{Lim} needed to satisfy the requirement. In our case, we chose a capacitance of 100 μF to make the overvoltage spike negligible. Figure 6 shows the behaviour after the short to ground is released. As can be seen, there is a very small overvoltage, due to the presence of a very small series inductance within the selected capacitance (metalized polypropylene). The small equivalent series resistance (ESR) and series inductance of such capacitors are essential to satisfy (1). The small oscillation due to the continuous exchange of energy between the capacitance and the inductance of the cable is soon dissipated by the series resistance of the cable and the load impedance in parallel to the capacitance itself. The same approach was used at the input of the DC/DC, where a metalized polypropylene 68 μF capacitor was used.

The filter is shown in Figure 7. At the input of the filter is a common mode choke that cancels the common mode signal disturbances. Four capacitors are then connected between the output and ground. C_P is a metalized polypropylene capacitor, with the main purpose of protecting against overvoltage, but also of filtering at high frequency due to its low ESR and series inductance. C_F is a very large value electrolytic chosen to filter low frequency noise. C_{H1} and C_{H2} are of smaller value, chosen to be efficient at high frequency. Figure 8 shows a photograph of the protection/filter circuit, implemented on a PCB housed in a metallic box of $16 \times 16 \times 12$ cm^3.

One important remark is due at this point. When loading a voltage source with a large value capacitance with small ESR, possible instabilities can arise since the loop gain margin is degraded. To avoid this a very small series resistance should be present in series with the capacitance. This precaution is not needed if a long cable is used, as in our case, since its small series resistance is enough to prevent instabilities.
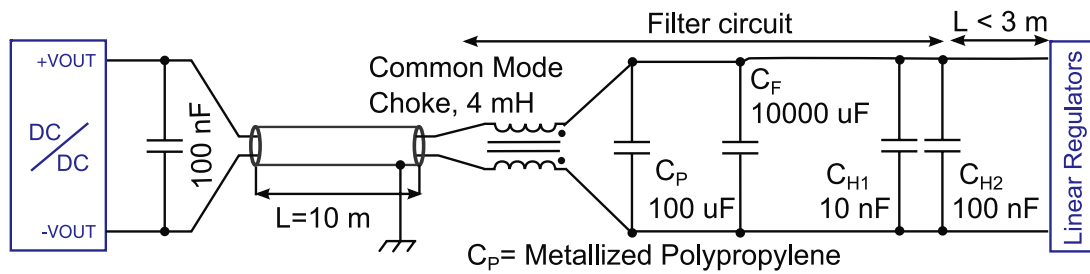
FIG. 7. Schematic of the protection/filter.

III. SYSTEM CHARACTERIZATION

The power slots have been produced in 30 units to face the needs of CUORE. They have all been characterized in static and noise performances. The efficiency of our protection/filter circuit has been validated with both the power slots and the commercial medium-power AC/DC.

A. Static performance of the power slots

Each power slot module was tested at a load current in excess of about 30% of that expected in operating conditions. A power 1 Ω resistor was connected at the output and the voltage was regulated to about 7.5 V to set the current at 7 A. This test condition was maintained for 24 h and current, voltage, and temperature were monitored every 30 s. All the modules worked properly and a summary of the results is shown in Figure 9, where the histogram distribution of the thermal drift is shown. This distribution is quite rough since the temperature of the environment changed only by few degrees during the day and the ADC resolution of the μcontroller is 12 bits, or 500 ppm at 7.5 V. The average drift is zero, with a spread of about ± 2000 ppm/$°$C or $\pm 0.2\%$/$°$C.

The temperature of the power slot rises to 70 $°$C if no fan is used, in the above operating conditions. The use of a tangential blower (QL4/1500-2112 from Ebmpapst, 50 m^3/h) below the boards allowed to maintain the temperature at 40 $°$C. The tangential blower minimizes the injection of magnetic disturbances towards the boards, being the air flux orthogonal to the rotational axis.

B. Noise measurement

The achievement of low noise in high power supply systems must take into account non-negligible effects coming from any possible small fluctuation of the impedance in the signal path. To consider an example, if the output current of a voltage supply is 10 A and in any part of the link between the source and the load there is an impedance fluctuation of the order of only 1 $\mu\Omega$, a change of 10 μV is expected across the load. The sources of such noise are normally located at the connector contacts, induced by mechanical vibrations which, consequently, confine the effects of these disturbances to low frequency. A workaround to these effects is to distribute the power with several sources in order to lower the driving current from each source, or to use very stable connectors like in our case (see the left of Figure 8).

Another source of noise are the protecting fuses. Some fuse types, especially when the tripping current of the fuse is not far from the working conditions, can give small changes of the fuse impedance which result in low frequency noise. This comes from the fact that a fuse has an impedance that is negligible till it gets close to the tripping current, where it increases very suddenly. An example is shown in Figure 10. The large number of slow pulses due to the fuse are clearly evident. See the following Figure 13, taken without the fuse, for comparison.

A last source of non-fundamental noise is microphonism, or disturbances coming from the mechanical vibration of the cables. These are related with changes in the energy stored in the cables that is proportional to the output current (through the cable inductance) and to the cable capacitance. The effects of microphonism are mitigated by shielding the cables with a copper mesh, in order to minimize the capacitance variations.
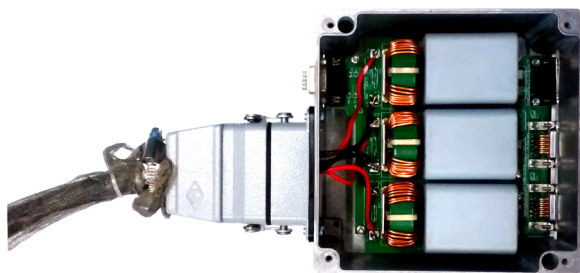

FIG. 8. Photograph of the protection/filter with the 10 m cable from the DC/DC connected at its input. Three common mode chokes with three sets of capacitors can be seen. The sides of the box are 12 cm long.
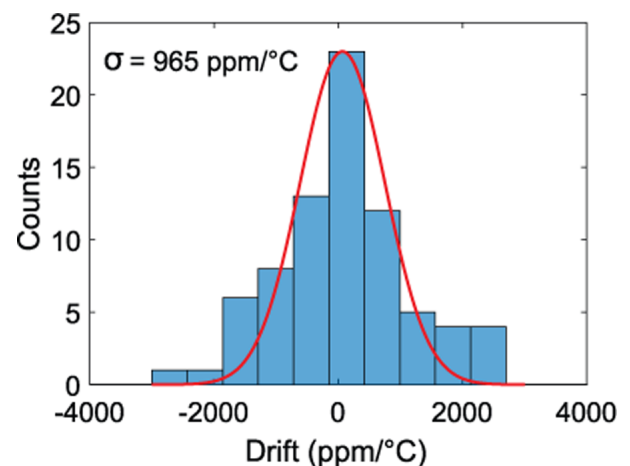

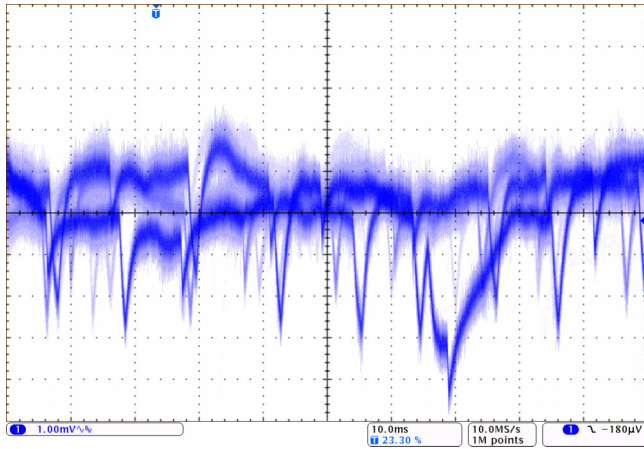FIG. 9. Thermal drift distribution of the DC/DC.

FIG. 10. Screenshot taken at the output of the amplifier (see below for its description) with a power slot connected at its input, when a fuse with a tripping current of just a few A above the operating current is in series with the source. The horizontal scale is 10 ms/div and the vertical scale is 1 mV/div at the amplifier output that corresponds to 11 μV/div at its input.

All the modules from our production were tested for noise performance. The measurements were performed at the output of the protection/filter. The setup used consisted in an amplifier followed by a spectrum analyzer (Agilent AG4395A), as shown in Figure 11. The two outputs of the Power Slot that are used for the analogue supply of the following Linear Power Supplies, DCDC$_1$ and DCDC$_2$ in the figure, were connected to the non-inverting input of the amplifier through the network composed by C$_{DUT}$, R$_{DUT}$, and R$_s$. Above a few Hz, such network attenuates the noise of each of the two DC/DCs by a factor of 3 (C$_{DUT}$ is 1000 μF, paralleled by 100 nF and 10 nF, R$_{DUT}$ is 50 Ω and the R$_s$ composition is 50 Ω as well).

The transfer function of the system is measured by injecting the signal V$_s$ through the switch SW$_1$ and the attenuator R$_{s1}$, R$_{s2}$ (50 Ω and 1 Ω). The amplifier is a non-inverting amplifier AC coupled from about 7 Hz (C$_A$ is 2200 μF paralleled by 100 nF and 10 nF, and R$_A$ is 10 Ω). We used a current feedback amplifier (AD811) for its wide bandwidth; its feedback impedance Z$_B$ was optimized for low noise in various frequency regions. More details on the amplifier and on the measurement technique are given in a referenced paper.[11] The amplifier was mounted on a small PCB located in the protection/filter box to minimize the length of its connections. This setup allowed to investigate noise from 10 Hz to 100 MHz, a bandwidth that largely exceeds the standard 20 MHz that is usually considered in this kind of characterization. The choice of such a large bandwidth ensures that all harmonics and disturbances up to very high frequency are taken into account and constitutes a
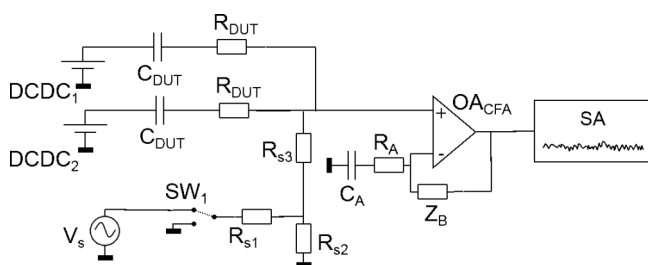
safety margin in assessing the low noise performance of the system.

C. Noise of the DC/DC power slot

All DC/DCs were operated at 7 A. We measured the noise N according to the setup of Figure 11 and referred the spectra to each Power Slot, assuming that

$$N_{Power\ Slot}^2 \approx \frac{(N_{DCDC1}^2 + N_{DCDC2}^2)}{2}. \tag{2}$$

The measured noise level and its uniformity between the modules were extremely satisfactory. In Figure 12, the superposition of all the noise spectra is shown. The spectra are all very close to each other. A color was assigned to each spectrum following a thermal color scale based on the RMS value, shown on the right side of the figure.

The low frequency noise is small, about 0.5 μV/$\sqrt{\text{Hz}}$ at 10 Hz. Up to 10 KHz the RMS noise is only about 2.7 $^{-0.3}_{+0.4}$ μV. The noise above a few KHz is limited by the OA_{CFA} amplifier to a few nV/$\sqrt{\text{Hz}}$. We subtracted it from the total measured noise to obtain the RMS noise of the DC/DC (protection/filter included) which up to 50 MHz is 15.5 $^{-6.5}_{+14.5}$ μV, while in the full 100 MHz investigated bandwidth results in 37 $^{-12}_{+11}$ μV. The larger spread in the RMS at high frequency is due to the presence of spurious high frequency peaks in some noise spectra, that we attributed to EMI disturbances rather than switching noise, since the latter in our DC/DC modules has a frequency that ranges from 20 KHz to 800 KHz.

The dashed green curve in Figure 12 is the fitting curve of the average of all the measured spectra. The fitting curve is given by

$$N^2 = \frac{a_f}{1 + (f/f_f)^{b_f}} + w. \tag{3}$$

In the above equation, w is the white, or high frequency, noise, while the first term accounts for the Low Frequency Noise, LFN. Following the classical theory[12,13] LFN is due to trapping/de-trapping centers for charge carriers. This random

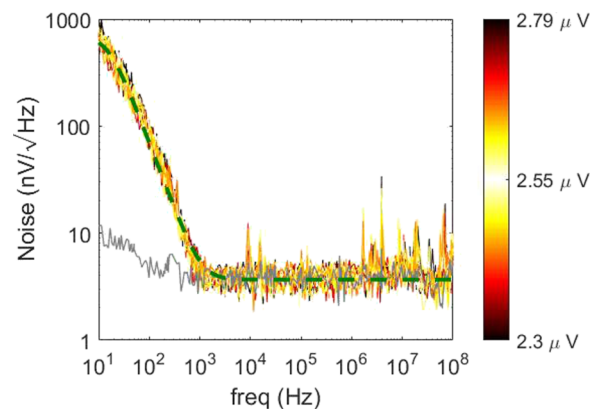FIG. 11. Circuit setup for noise measurements.

FIG. 12. Superposition of the noise spectra of 30 power slots (60 DC/DCs) operated at 7 A. The curves are barely distinguishable. A thermal scale is used to color the lines, labeled after their RMS noise calculated up to 10 KHz. The dashed green curve is the fit of the average spectrum. The noise floor of the second stage amplifier is shown in grey.
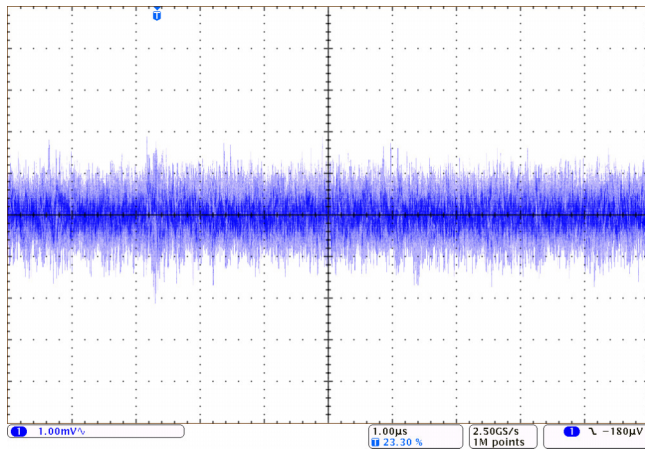
FIG. 13. Screenshot taken at the output of the amplifier with a power slot connected at its input. The horizontal scale is 1 μs/div and the vertical scale is 1 mV/div at the amplifier output that corresponds to 11 μV/div at its input.

mechanism is well described, in time domain, by exponential functions which have as their counterparts, in the frequency domain, Lorentzian functions, namely the first term of (3) when b_f has the value of 2. If several different centers are present the superposition of Lorentzian functions must be considered and their convolution is generally well fitted by a simplified $1/f$ dependence. Since, in our case, several low pass filters are present between the noise sources and the measured node, the original noise mechanisms are "deformed" and we obtain a good empirical fit employing one Lorentzian function whose power term b_f was left free to change.

Noise analysis was as follows. First all the noise spectra were fitted with (3) with all the 4 parameters free to change. Then we ran the fits again, but with the parameters responsible for the shape, namely f_f and b_f, fixed to the average values found previously. The average for f_f resulted 15.7 Hz, that for b_f 2.47. The new fits had only 2 free parameters, the LFN coefficient a_f and the white noise term w. The average value of a_f resulted in $3.9\,^{-0.9}_{+1.9} \times 10^{-13}$ V^2/Hz, while that of w $1.40\,^{-0.08}_{+0.12} \times 10^{-17}$ V^2/Hz.

In Figure 12, the noise of the amplifier used for noise measurements (OA_{CFA} of Figure 11) is shown in grey. This time the LFN coefficient a_f is only 0.53×10^{-17} V^2/Hz, totally negligible compared to the LFN of the DC/DCs, while the white noise, w, is 1.42×10^{-17} V^2/Hz ($f_f = 14.2$ Hz, $b_f = 2,55$). White noise is equal to that measured with the DC/DCs connected and this proves the good performance of the low pass filtering. The RMS noise of the DC/DCs results to be larger than that of the amplifier, mainly due to EMI disturbances coming from the environment. These disturbances are detectable almost only in the frequency domain, as can be observed in Figure 13, where the screenshot of the noise at the output of the amplifier is shown. Once referred to the amplifier input, namely, the DC/DC output, the vertical scale is about 11 μV/div. The noise here is that of the DC/DC summed to that of the amplifier over a bandwidth of a few MHz, since the horizontal scale is 1 μs/div. No clear evidence of switching disturbances from the DC/DC are visible.

Noise from DC/DCs was found to be only slightly dependent on the output current and Figure 14 shows this for
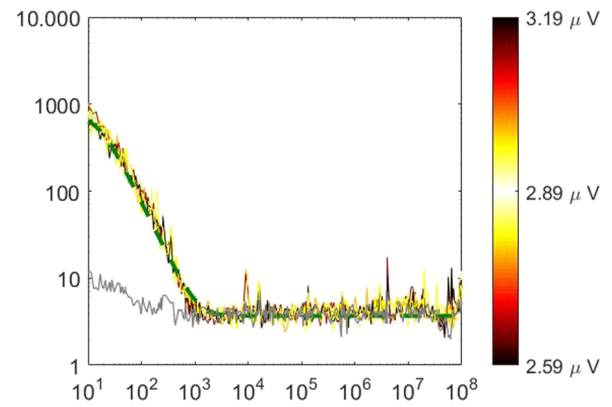

FIG. 14. Superposition of the noise spectra from a DC/DC unit at the different load currents of 6 A, 7 A, 8 A, 9 A, and 10 A. The curves are barely distinguishable. A thermal scale is used to color the lines, labeled after their RMS noise calculated up to 10 KHz. The dashed green curve is the fit of the average spectrum. The noise floor of the second stage amplifier is shown in grey.

one DC/DC operated at 6 A, 7 A, 8 A, 9 A, and 10 A. The spectra are so close that telling them apart is almost impossible, so no labels were added. The color code is again related with the RMS noise up to 10 KHz. The fits were computed based on (3), but with the shape parameters f_f and b_f fixed as was done for Figure 12. The noise coefficient a_f resulted in $5.9\,^{-1.1}_{+1.7} \times 10^{-13}$ V^2/Hz, and w resulted in $1.41\,^{-0.067}_{+0.58} \times 10^{-17}$ V^2/Hz.

D. Noise of the AC/DC HMP4040

The HMP4040 AC/DC shows a higher LFN, as can be observed in Figure 15 where the noise was measured at different loading currents, 5 A, 6.7 A, 8.4 A, and 9 A, at the output of our protection/filter. Again, the noise is almost independent of the load current. Once again, we fitted the spectra leaving all the parameters of (3) free; then we fixed f_f at the average value of 51 Hz and b_f at 2.63. Since several peaks due to switching disturbances were found in the spectra, we fixed also the white noise w at 1.4×10^{-17} V^2/Hz. The resulting LFN coefficient a_f was $7.3\,^{-0.91}_{+1.81} \times 10^{-11}$ V^2/Hz. The
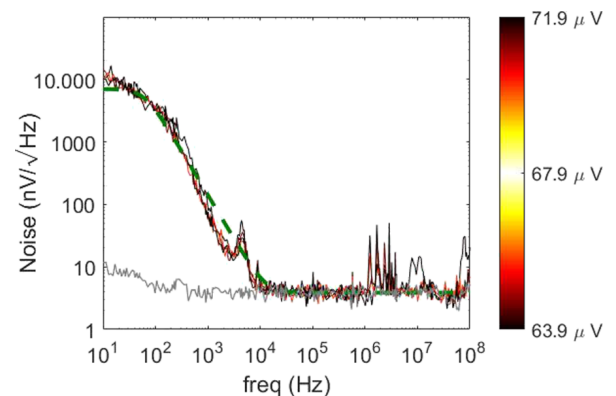

FIG. 15. Superposition of the noise spectra from a HMP4040 at the different load currents of 5 A, 6.7 A, 8.4 A, and 9 A. The curves are barely distinguishable. A thermal scale is used to color the lines, labeled after their RMS noise calculated up to 10 KHz. The dashed green curve is the fit of the average spectrum. The noise floor of the second stage amplifier is shown in grey.
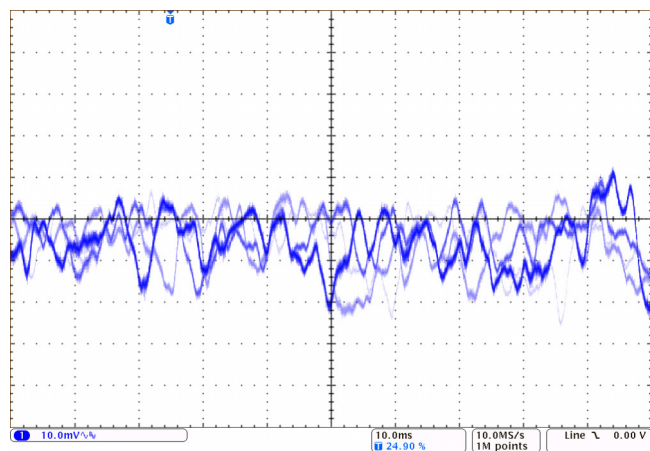
FIG. 16. Screenshot taken at the output of the amplifier with a HMP4040 loaded with 7 A connected at its input. The horizontal scale is 10 ms/div and the vertical scale is 10 mV/div at the amplifier output that corresponds to 120 μV/div at its input.

RMS noise in the first 10 KHz was about $68\,^{-4.00}_{+9.43}\,\mu$V and did not change much going to the full bandwidth of 100 MHz, where it became $90\,^{-19}_{+51}\,\mu$V.

Figure 16 shows the scope screenshot of the output of the amplifier when the HMP4040 loaded with 7 A is connected at its input through the protection/filter. The peak-to-peak noise of the HMP4040, after the protection/filter, is lower than 0.5 mV. This performance is worse than that of the power slot DCDCs presented in this paper, but it is anyway remarkable when compared to standard power supply noise figures. The picture is interesting as it clearly shows the LFN in time domain.

IV. CONCLUSIONS

The design choices and the measured performance of the power supply systems for the CUORE and LUCIFER experiments were presented. In the case of CUORE, a careful design of the DC/DC modules and filters allowed to reach a noise level of 37 μV RMS from 10 Hz to 100 MHz. The modules also show a thermal drift below ±0.2%/°C. These results were found consistent over the entire production lot of 30 modules. In the case of LUCIFER, based on a simpler commercial solution, proper filtering allowed to keep the RMS noise below 100 μV in the same bandwidth. The noise filters also provide protection in case of inductive spikes in the long connecting cables. A negligible dependence on the output currents was found in both cases.

[1]C. Arnaboldi *et al.* (CUORE Collaboration), Nucl. Instrum. Methods Phys. Res., Sect. A **518**, 775 (2004).
[2]D. Artusa *et al.* (CUORE Collaboration), Eur. Phys. J. C **74**, 3096 (2014).
[3]J. W. Beeman *et al.*, Adv. High Energy Phys. **2013**, 237973.
[4]L. Cassina, A. Giachero, C. Gotti, M. Maino, and G. Pessina, in IEEE Nuclear Science Symposium Conference Record, NPO2.71, 2013.
[5]G. Pessina, Rev. Sci. Instrum. **70**, 3473 (1999).
[6]Vicor Design Guide & Applications Manual, 2014.
[7]Vicor Application Note: Noise-Related Performance Comparison of Two DC-DC Converter Topologies, 2009.
[8]R. Marchetti, Electronics Design, Strategy, News (EDN) 2007.
[9]Vicor Application Note: DC-DC Converters Design Guide, 2005.
[10]Vicor MicroRam datasheet, 2014.
[11]P. Carniti, L. Cassina, C. Gotti, M. Maino, and G. Pessina, J. Instrum. **10**, P08016 (2015).
[12]A. V. D. Ziel, in *Fluctuation Phenomena in Semiconductors* (Butterworth Scientific Publications, 1959), Chaps. 4 and 5.
[13]A. V. D. Ziel, in *Noise in Solid State Devices and Circuits* (Wiley Interscience, 1986), Chaps. 7 and 8.